VIP Nanomaterials

DOI: 10.1002/anie.201203207

Synthesis of Monolayer-Patched Graphene from Glucose**

Xin-Hao Li, Simon Kurasch, Ute Kaiser, and Markus Antonietti**

The extraordinary electronic and mechanical properties[1,2] of graphene have stimulated intense research on developing simple methods for the large-scale synthesis of graphene.[1–9] High-quality large-area graphene films prepared by the chemical vapor deposition of various carbon-containing molecules on arbitrary substrates could meet the requirements of large-area electronic applications.[3–7] For the industrial production of conductive graphene powder on the ton scale,[3,9,11–13] the chemical exfoliation of graphite minerals still remains the main manufacturing path.[3,8–10] On the other hand, the exclusive two-dimensional polymerization of graphene-like structures from simple monomers still presents a challenge for carbon chemists.[14–19] Further fine-tuning of the Fermi level of graphene by doping offers a way to control the electronic structure of carbonaceous materials[6,20–23] and is of major interest for their application in electronics, electrodes, and catalysis. The electronic properties of doped graphene are strongly linked to the dopant concentration,[24] which is only poorly controlled by current methods. It is therefore highly challenging but desirable to develop effective approaches for fabricating graphene that is cheap yet of high quality (e.g. high surface area, high conductivity, doping level, and uniform morphology) in a controlled manner.

Herein we report a simple yet versatile approach for the synthesis of two-dimensional (2D) carbon materials ranging from free-standing monolayers to oligolayered graphene by the calcination of glucose, a most abundant, sustainable compound. In this synthesis only dicyandiamide (DCDA) was added for the temporary in situ formation of layered graphic carbon nitride ($g\text{-}C_3N_4$), which serves as a sacrificial template.[25,26] This approach is also facile for gradually tuning the concentration of the nitrogen dopant in a broader range without disturbing the morphology of graphene. In a typical synthesis, the two-step heating of a mixture of DCDA and glucose under a protective flow of N_2 directly resulted in free-standing graphene with a yield of 28–60% (calculated based on added carbon from glucose).

The overall formation process is depicted in Figure 1: Thermal condensation of DCDA creates a layered carbon nitride template (simplified as $g\text{-}C_3N_4$, see Figure S1 in the Supporting Information), which binds the as-formed aromatic carbon intermediates to its surface by means of donor–acceptor interactions and finally confines their condensation in a cooperative process to the interlayer gaps of $g\text{-}C_3N_4$ at 600 °C. The stacking heights of the two phases are controlled by the relative amounts of the two monomers, glucose and dicyandiamide. Since the $g\text{-}C_3N_4$ template undergoes complete thermolysis at 750 °C, the latest graphene-like sheets are liberated at higher temperatures (Figure S2 in the Supporting Information). Those obtained at 1000 °C contain minute amounts of nitrogen atoms (4.3 atom%) and are denoted as Gr.

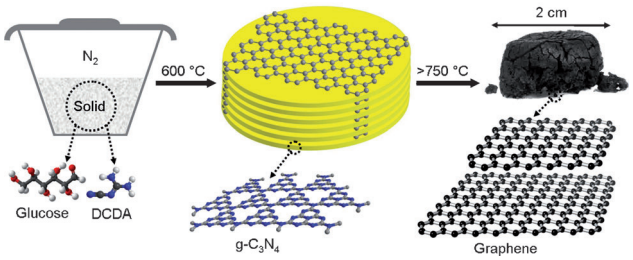

Figure 1. Proposed synthetic protocol for free-standing graphene. Bottom: Repetition motifs of an ideal $g\text{-}C_3N_4$ plane (middle) and of graphene (right); C black or gray, N blue.

Representative scanning electron microscopy (SEM) images (Figure 2a,b and Figure S3 in the Supporting Information) of as-synthesized samples at increasing magnification reveal a uniform, layered morphology on a larger scale. The graphitic samples are obtained as monoliths of continuous but entangled thin graphene sheets without any post-purification or separation processes. Unlike chemically reduced graphene obtained by heating graphene oxides or functionalized graphene at high temperatures, which usually undergo extended aggregation into thick flakes,[27] the primary nanosheets constituting the monoliths are thin and very flexible. The typical wrinkles of free-standing monolayers or oligolayered graphenes are observed in each of the tectonic units with overall sizes up to tens to hundreds of micrometers. It must be mentioned that the synthesis was not optimized to maximize the size of the graphene plates.

Since their thickness is in the sub-nanometer range, the graphitic monoliths could be easily torn and/or dispersed by mild ultrasonication in various solvents without the assistance

[*] Dr. X.-H. Li, Prof.Dr. M. Antonietti
Abteilung Kolloidchemie
Max-Planck-Institut für Kolloid- und Grenzflächenforschung
Wissenschaftspark Golm, 14424 Postdam (Germany)
E-mail: antonietti@mpikg.mpg.de
xin-hao.li@mpikg.mpg.de
Dr. S. Kurasch, Prof.Dr. U. Kaiser
Materialwissenschaftliche Elektronenmikroskopie
Zentrale Einrichtung Elektronenmikroskopie, Universität Ulm
Albert Einstein Allee 11, 89081 Ulm (Germany)

[**] This work was supported by the ENERCHEM project of the Max Planck Society and also by the Alexander von Humboldt Foundation.

Supporting information for this article (experimental details, more characterization results, and detailed discussions) is available on the WWW under http://dx.doi.org/10.1002/anie.201203207.

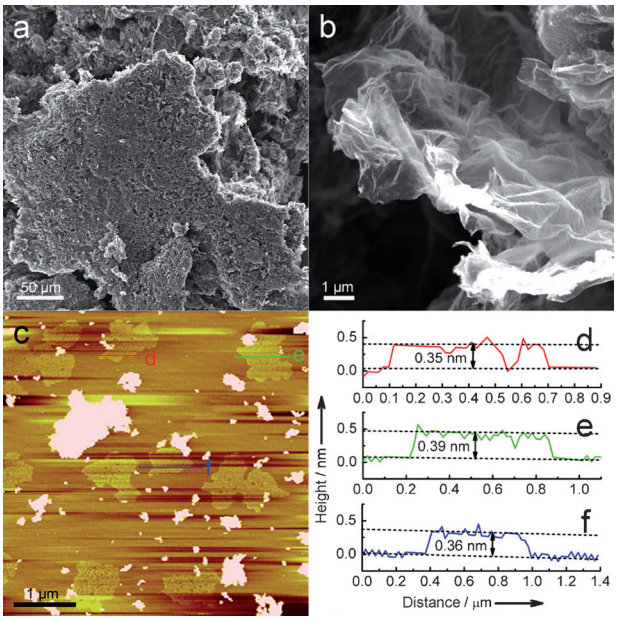

Figure 2. Microstructure of sample Gr. a,b) SEM images of the as-formed Gr sample with increasing magnification. c) AFM image of Gr sheets deposited on freshly cleaved mica from a DMF dispersion, and corresponding height measurements (d–f).

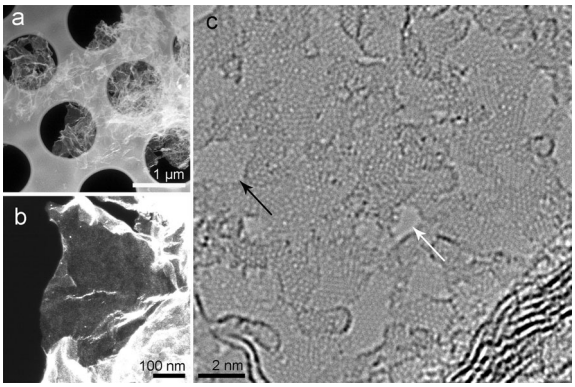

Figure 3. Dark-field and AC-HRTEM images of Gr sheets. a) Overview dark-field image of free-standing Gr sheets; the image is displayed on a square-root gray scale for better visibility of thin areas. b) Enlargement of a large, very thin, and very homogeneous section from (a) on a linear gray scale. c) HRTEM image of a similar area showing the graphene-like structure of the Gr sheet. Black arrow indicates single-layer patch with a grain boundary built from pentagon–heptagon pairs; this is similar to what is found in CVD graphene samples. The irradiation of the electron beam may generate new holes (marked within white arrow) i the plane.

of any stabilizer, because the adsorbed solvent molecules can act as a stabilizer.[28] Similar to highly reduced, graphene oxide monolayers,[29] our graphene samples show good dispersability in DMF and/or water, moderate dispersability in ethanol, and very poor dispersability in other solvents (Figure S4 in the Supporting Information). Figure S3 a and its inset show TEM images very typical for single-layer graphene: one can clearly see the homogeneous, sheetlike structure of the material and can exclude the presence of irregular particles or hollow structures (including carbon nanotubes and fullerenes) in the samples (Figure S5). It is also clear from the TEM images (Figures S5 and S6) that the graphene dispersion in the liquid medium contains both crumpled, entangled, three-dimensional network clusters and smaller, presumably fragmented, unfolded nanosheets. Ultra-flat, freshly cleaved mica can help to suppress the intrinsic corrugation of these monolayer graphene flakes.[30] AFM images (Figure 2 c–f) directly prove the presence of a layer structure of unfolded sheets on a mica substrate with a uniform layer thickness between 0.35 and 0.39 nm, matching well with the theoretical van der Waals thickness (0.34 nm) of ideal monolayer graphene. In Figure 2 c, we also see some stacked species with a thickness of tens to hundreds of nanometers. Here, the sharp but irregular edges indicate that the smaller flakes are torn by ultrasound from larger entities. More intense sonication results in more exfoliated but even smaller monolayer graphene nanosheets (Figure S6).

The real structure of the as-formed graphene nanosheets is nicely revealed by aberration-corrected high-resolution transmission electron microscopy (AC-HRTEM) observation at the atomic level.[31,32] The dark-field images (Figure 3 a,b) reveal the homogeneous thickness of the unfolded parts. Typical honeycomblike molecular structures (Figure 3 c and Figure S7) of hexagonally connected carbon atoms are evident in the unfolded part of the primary sheet, however, only with a restricted domain size. This is why we refer to these sheets as "nanocrystalline" or "patched" layers. Holes were formed by the irradiation of the electron beam during the HRTEM observation (Figure 3 c and Movies S1 and S2 in the Supporting Information), as is typical for a very thin carbon sample. Beside mono- and double-layer structures, also multilayered graphene domains are observed, but only as a smaller fraction of the sample. The primary graphene nanodomains, sized between 2 and 15 nm with irregular shapes and observable boundaries, are interconnected in the final mosaic films (Figure 3 c and Figure S7b). Two-dimensional "patched" graphene can be understood as a novel species between ideal graphene and amorphous carbon. A similar nanocrystalline structure of two-dimensional carbon has recently also been observed in graphene made by annealing ultrathin films of aromatic carbon sources on top of certain substrates in high vacuum at temperatures up to 900 °C.[19] Of course, such a substrate-based technique cannot provide the product in gram quantities, but nevertheless, the extraordinary electronic properties of two-dimensional "patched" graphene were already demonstrated there.[19]

X-ray diffraction (XRD) patterns (Figure S8a) indicate that the as-formed graphene flakes are composed of only graphitic carbon and do not contain impurities. A G-band at 1578 cm^{-1} in the 532 nm Raman spectrum (Figure 4 a) of the Gr sample also supports the formation of graphitic carbon. Similar to nanometer-sized graphite particles and chemically modified graphene flakes, the sample has also a broad D-band centered at 1.360 cm^{-1}, reflecting the presence of disorder and the edges and boundaries of the graphene domains, as already demonstrated by the AC-HRTEM observation. The sharp and asymmetrical C 1s peak (Figure 4 c) of the X-ray photoemission spectroscopy (XPS) spectra at 284.7 eV further

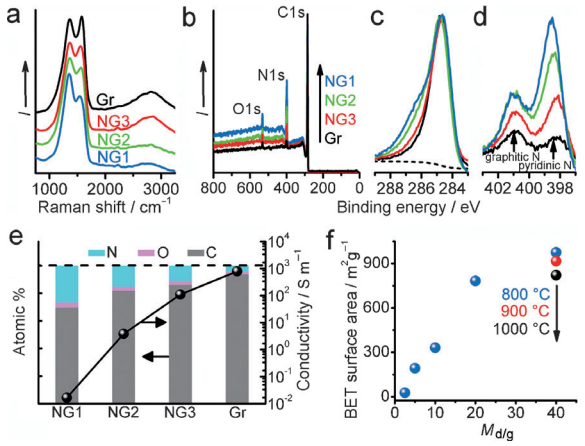

Figure 4. Raman spectra (a), XPS spectra (b), C 1s spectra (c), and N 1s spectra (d) of Gr and NG1–NG3. e) Content of C, N, and O atoms in Gr and NGs based on XPS analysis, and corresponding bulk conductivity (line and symbol). Dashed line: 100 atom% and bulk conductivity of crystalline graphite powder (1300 S m^{-1}), respectively. f) BET surface area of Gr and NG obtained from a mixed precursor with different $M_{d/g}$ values at 800 °C for 1 h (blue), or by heating the same precursor ($M_{d/g}$: 40) at 900 °C (red) or 1000 °C (black) for 1 h.

excludes significant modifications of the sp^2 carbon atoms in the graphene sample, i.e. the sample consists of essentially sp^2-hybridized carbon atoms. The total content (Figure 4e) of foreign atoms (including N and O) based on the XPS analysis (Figure 4b) is less than 7 atom%, part of which is in the form of surface-absorbed water and other small molecules, as reflected also by the thermogravimetric analysis (TGA, Figure S8b), which shows a sample weight loss of 4.2% below 180 °C. One must be very clear that such high-surface-area aromatic carbon are superadsorbing. This means clean samples exist only in high vacuum; under any other environmental conditions gases, carbon dioxide, or water are immediately adsorbed in larger amounts. All these characterizations support the well-developed character of graphene domains over the whole sample.

The as-fabricated monoliths of patched graphene (Figure 1, top right) are extremely lightweight with a foam density of 0.0077 g cm^{-3} and a very high specific surface area of 820 m^2 g^{-1} (Figure 4f and Figure S9), corresponding to a calculated average number of layers of three (over the complete sample). The high surface area of the sample is comparable with that of CVD-generated graphene networks (850 m^2 g^{-1}, density of 0.005 g cm^{-3}) on Ni foam,[33] and is higher than those of highly reduced graphene oxides and solvothermally synthesized graphene assemblies.[9,15] Despite the high surface area and multiple interfaces, the bulk conductivity (Figure 4e) of the graphene powder is as high as 785 S m^{-1}, which agrees very well with the measured values of CVD-generated graphene networks with an average number of three layers.[33] It seems that the myriad boundaries in the mosaic graphene planes do not significantly disturb the electrical conductivity. On the contrary, the large-area and partially interconnected mosaic graphene sheets seem to improve the electrical conductivity, which supports their direct use in composite materials for electrical applications.

The specific surface area and thus the average number of graphene layers can be tuned by varying the DCDA/glucose mass ratio ($M_{d/g}$). When $M_{d/g}$ was tuned from 40 to 10, the specific surface area of these samples decreased from 975, to 782 and finally to 331 m^2 g^{-1} (Figure 4f and Figure S9) and the average number of graphene layers of the resulting stacks increased from three to about eight. The minimum value of $M_{d/g}$ for the formation of layered graphene flakes is around 10 (Figure S10). When the $M_{d/g}$ value was too low (≤ 5), only spongelike mesoporous, 3D-interconnected, graphitic carbon resulted.

The described synthesis also demonstrates the potential of controlling the dopant concentration and the microstructure of the graphene materials by chemical means. The nitrogen content of the graphene nanosheets already at this elemental stage is controlled by the heating temperature and reaction time (see Table S1). The introduction of N atoms in the graphene plane results in an increased intensity ratio of the D- and G-bands in the Raman spectrum (Figure 4a), and XPS analysis (Figure 4c) reveals that the nitrogen content decreases from 26.8 atom% to 4.3 atom% when the reaction temperature and/or time is increased. The variation of the N content indeed changes the properties of the as-formed graphene samples. For example, the bulk conductivity of NG1 (N content: 26.8 atom%) is only 0.017 S m^{-1}, 5 orders of magnitude lower than that of Gr. The high surface specific area of NG1 (975 m^2 g^{-1}, Figure S8), the highly separated morphology of the NG1 sheets based on SEM observation (Figure S11a–c), and the TGA results (Figure S2) unambiguously exclude the presence of residues of the carbon nitride template in the NG1 sample.

The N 1s XPS peak (Figure 4d and Figure S11d) of the samples further indicate that the N atoms are inserted into the graphene lattice mainly in the form of "pyridinic" N and a minor amount of "graphitic" N atoms, that is, in-plane. The decrease in conductivity can be mainly attributed to the increased content of "pyridinic" N atoms.[21] Unlike the postannealing of as-formed graphene in NH_3, which usually results in N doping at the edges and defect sites, a certain amount of "graphitic" N atoms (>10%) is found in all these samples. The relative contribution of "graphitic" N atoms also increases with the synthesis temperature. Moreover, the heating temperature has only a slight effect on the morphology and the surface area of the as-formed graphene or N-doped graphene (Figure 4f). Both the uniform structure and the high surface specific area of the samples were maintained when the reaction temperature was varied from 1000 to 800 °C. Considering the ambipolar electric field effect observed in nanocrystalline graphene, our synthetic approach for fabricating graphene samples with tunable dopant concentrations should pave the way for some refined electronic applications. The resulting graphene or N-doped graphene monoliths were, for instance, used as electrocatalysts for the oxygen reduction reaction (ORR) (Figure S12). Gr showed superior activity and remarkably good tolerance to fuel crossover effects.

Given that this synthetic technique utilizes cheap precursors and does not require organic solvents, catalysts, substrates, vacuum systems, or post-purification processes, the

mass production of highly conductive graphene materials with high surface specific area can be envisaged at acceptable costs. The facile incorporation of dopants into highly conjugated graphene planes combined with their excellent accessibility can promote the practical application of these graphene materials as efficient and stable cathode materials, catalysts, and nanofillers. Moreover, the unique boundary-rich patched graphenes may increase specific possibilities to functionalize the graphene by chemical modification and thus promise new properties and applications for nanocarbon materials.

Received: April 26, 2012
Published online: August 21, 2012

Keywords: conducting materials · glucose · graphene · materials science · nanostructures

[1] K. S. Novoselov, A. K. Geim, S. V. Morozov, D. Jiang, Y. Zhang, S. V. Dubonos, I. V. Grigorieva, A. A. Firsov, *Science* **2004**, *306*, 666 – 669.
[2] A. K. Geim, K. S. Novoselov, *Nat. Mater.* **2007**, *6*, 183 – 191.
[3] M. J. Allen, V. C. Tung, R. B. Kaner, *Chem. Rev.* **2010**, *110*, 132 – 145.
[4] X. S. Li, W. W. Cai, J. An, S. Kim, J. Nah, D. X. Yang, R. Piner, A. Velamakanni, I. Jung, E. Tutuc, S. K. Banerjee, L. Colombo, R. S. Ruoff, *Science* **2009**, *324*, 1312 – 1314.
[5] K. S. Kim, Y. Zhao, H. Jang, S. Y. Lee, J. M. Kim, K. S. Kim, J.-H. Ahn, P. Kim, J.-Y. Choi, B. H. Hong, *Nature* **2009**, *457*, 706 – 710.
[6] Z. Z. Sun, *Z.* Yan, J. Yao, E. Beitler, Y. Zhu, J. M. Tour, *Nature* **2010**, 468, 549 – 552.
[7] F. Schwierz, *Nat. Nanotechnol.* **2010**, *5*, 487 – 496.
[8] W. S. Hummers, R. E. Offeman, *J. Am. Chem. Soc.* **1958**, *80*, 1339.
[9] S. Park, R. S. Ruoff, *Nat. Nanotechnol.* **2009**, *4*, 217 – 224.
[10] S. Stankovich, D. A. Dikin, R. D. Piner, K. A. Kohlhaas, A. Kleinhammes, Y. Y. Jia, Y. Wu, S. T. Nguyen, R. S. Ruoff, *Carbon* **2007**, *45*, 1558 – 1565.
[11] S. Stankovich, D. A. Dikin, G. H. B. Dommett, K. M. Kohlhaas, E. J. Zimney, E. A. Stach, R. D. Piner, S. T. Nguyen, R. S. Ruoff, *Nature* **2006**, *442*, 282 – 286.
[12] M. Segal, *Nat. Nanotechnol.* **2009**, *4*, 612 – 614.
[13] Y. W. Zhu, S. Murali, M. D. Stoller, K. J. Ganesh, W. W. Cai, P. J. Ferreira, A. Pirkle, R. M. Wallace, K. A. Cychosz, M. Thommes, D. Su, E. A. Stach, R. S. Ruoff, *Science* **2011**, *332*, 1537 – 1541.
[14] Y. P. Zhai, Y. Q. Dou, D. Y. Zhao, P. F. Fulvio, R. T. Mayes, S. Dai, *Adv. Mater.* **2011**, *23*, 4828 – 4850.
[15] M. Choucair, P. Thordarson, J. A. Stride, *Nat. Nanotechnol.* **2009**, *4*, 30 – 33.
[16] J. S. Wu, W. Pisula, K. Müllen, *Chem. Rev.* **2007**, *107*, 718 – 747.
[17] J. M. Cai, P. Ruffieux, R. Jaafar, M. Bieri, T. Braun, S. Blankenburg, M. Muoth, A. P. Seitsonen, M. Saleh, X. F. Feng, K. Müllen, R. Fasel, *Nature* **2010**, *466*, 470 – 473.
[18] L. Dössel, L. Gherghel, X. L. Feng, K. Müllen, *Angew. Chem.* **2011**, *123*, 2588 – 2591; *Angew. Chem. Int. Ed.* **2011**, *50*, 2540 – 2543.
[19] A. Turchanin, D. Weber, M. Büenfeld, C. Kisielowski, M. V. Fistul, K. B. Efetov, T. Weimann, R. Stosch, J. Mayer, A. Gölzhäuser, *ACS Nano* **2011**, *5*, 3896 – 3904.
[20] X. R. Wang, X. L. Li, L. Zhang, Y. Yoon, P. K. Weber, H. L. Wang, J. Guo, H. J. Dai, *Science* **2009**, *324*, 768 – 771.
[21] X. L. Li, H. L. Wang, J. T. Robinson, H. Sanchez, G. Diankov, H. J. Dai, *J. Am. Chem. Soc.* **2009**, *131*, 15939 – 15944.
[22] D. C. Wei, Y. Q. Liu, Y. Wang, H. L. Zhang, L. P. Huang, G. Yu, *Nano Lett.* **2009**, *9*, 1752 – 1758.
[23] L. T. Qu, Y. Liu, J.-B. Baek, L. M. Dai, *ACS Nano* **2010**, *4*, 1321 – 1326.
[24] L. Y. Zhao, R. He, K. T. Rim, T. Schiros, K. S. Kim, H. Zhou, C. Gutiérrez, S. P. Chockalingam, C. J. Arguello, L. Pálová, D. Nordlund, M. S. Hybertsen, D. R. Reichman, T. F. Heinz, P. Kim, A. Pinczuk, G. W. Flynn, A. N. Pasupathy, *Science* **2011**, *333*, 999 – 1003.
[25] A. Thomas, A. Fischer, F. Goettmann, M. Antonietti, J.-O. Müller, R. Schlögl, J. M. Carlsson, *J. Mater. Chem.* **2008**, *18*, 4893 – 4908.
[26] X.-H. Li, J.-S. Chen, X. C. Wang, J. H. Sun, M. Antonietti, *J. Am. Chem. Soc.* **2011**, *133*, 8074 – 8077.
[27] Z. H. Sheng, L. Shao, J.-J. Chen, W.-J. Bao, F.-B. Wang, X.-H. Xia, *ACS Nano* **2011**, *5*, 4350 – 4358.
[28] X.-H. Li, J.-S. Chen, X. C. Wang, M. E. Schuster, R. Schlögl, M. Antonietti, *ChemSusChem* **2012**, *5*, 642 – 646.
[29] S. Park, J. An, I. Jung, R. D. Piner, S. J. An, X. S. Li, A. Velamakanni, R. S. Ruoff, *Nano Lett.* **2009**, *9*, 1593 – 1597.
[30] A. Sinitskii, D. V. Kosynkin, A. Dimiev, J. M. Tour, *ACS Nano* **2010**, *4*, 3095 – 3102.
[31] A. Chuvilin, E. Bichoutskaia, M. C. Gimenez-Lopez, T. W. Chamberlain, G. A. Rance, N. Kuganathan, J. Biskupek, U. Kaiser, A. N. Khlobystov, *Nat. Mater.* **2011**, *10*, 687 – 692.
[32] J. Kotakoski, A. V. Krasheninnikov, U. Kaiser, J. C. Meyer, *Phys. Rev. Lett.* **2011**, *106*, 105505.
[33] Z. P. Chen, W. C. Ren, L. B. Gao, B. L. Liu, S. F. Pei, H.-M. Cheng, *Nat. Mater.* **2011**, *10*, 424 – 428.

